Applied Geochemistry 109 (2019) 104401

Contents lists available at ScienceDirect

Applied Geochemistry

journal homepage: www.elsevier.com/locate/apgeochem

Mobilisation of arsenic, selenium and uranium from Carboniferous black shales in west Ireland

Joseph G.T. Armstrong[a,*], John Parnell[a], Liam A. Bullock[a,b], Adrian J. Boyce[c], Magali Perez[d], Jörg Feldmann[d]

[a] School of Geosciences, University of Aberdeen, Meston Building, Aberdeen, AB24 3UE, UK
[b] Ocean and Earth Science, National Oceanography Centre Southampton, University of Southampton Waterfront Campus, European Way, Southampton, SO14 3ZH, UK
[c] Scottish Universities Environmental Research Centre, University of Glasgow, Rankine Avenue, Scottish Enterprise Technology Park, East Kilbride, Glasgow, G75 0QF, UK
[d] Trace Element Speciation Laboratory, School of Natural and Computing Science, University of Aberdeen, Meston Building, Aberdeen, AB24 3UE, UK

ARTICLE INFO

Editorial handling by Prof. M. Kersten

Keywords:
Black shale
Carboniferous
Regolith
Secondary mineralisation
Oxidation
Jarosite
Groundwater
Leaching
Fixation
Hydraulic fracturing
AMD
Selenium
Arsenic
Uranium
Critical elements

ABSTRACT

The fixation and accumulation of critical elements in the near surface environment is an important factor in understanding elemental cycling through the crust, both for exploration of new resources and environmental management strategies. Carbonaceous black shales are commonly rich in trace elements relative to global crustal averages, many of which have potential environmental impacts depending on their speciation and mobility at surface. This trace element mobility can be investigated by studying the secondary mineralisation (regolith) associated with black shales at surface. In this study, Carboniferous shales on the west coast of Ireland are found to have higher than average shale concentrations of As, Cd, Cu, Co, Mo, Ni, Se, Te and U, similar to the laterally equivalent Bowland Shales, UK. Groundwater penetration and oxidative weathering of these pyritic black shales produces oxide deposits, dominated by goethite and jarosite, which are significantly enriched in As (44–468 ppm), Se (12–184 ppm), U (6–158 ppm) and other trace elements, compared to concentrations in the parent shales. Major elemental abundances vary in composition from 3.5 to 29.4% sulphate, 0.6–9.1% phosphate and 36.6–47.2% iron-oxide. Phosphate substitution within jarosite is observed in these samples, formed under ambient pressure and temperature conditions.

The major and trace elements forming these secondary deposits are predominantly sourced from the underlying black shales through mobilisation by groundwater. This discovery is critical for the environmental assessment of black shale lithologies during shale gas exploration and production, where the demonstrated mobility of *in situ* elemental enrichments may indicate a significant source of produced- and groundwater contamination during and after hydraulic fracturing processes. The proportions of the major oxide phases exhibit a clear control on the trace elemental enrichments within the secondary deposits, where increasing Se and As concentrations correlate with increasing phosphate content of the jarosite mineralisation. This has implications for the remediation of acid mine drainage seeps, where phosphate-rich jarosite phases could be utilised for more efficient trace element removal.

1. Introduction

Carbonaceous sedimentary rocks are commonly enriched in redox sensitive trace elements, relative to average crustal abundances (Hu and Gao, 2008; Turekian and Wedepohl, 1961), including selenium (Se), arsenic (As), molybdenum (Mo), uranium (U), copper (Cu) and tellurium (Te). These elements are either of environmental concern, or economic importance, with Se, As, Mo and U considered environmentally hazardous in elevated concentrations (Bajwa et al., 2017; Hakonson-Hayes et al., 2002; Zheng et al., 1999) and Cu, Te, Se and Mo of increasing economic value in modern technologies (Cucchiella et al., 2015). Surface oxidation of pyritic carbonaceous lithologies, particularly coals, has long been recognised as environmentally hazardous, in part due to the liberation of toxic trace elements, including As and Se (Baruah and Khare, 2010; He et al., 2002; Wayland and Crosley, 2006). As such, understanding the mobility of trace elements resident in organic rich sedimentary rocks at surface and the potential mechanisms for their fixation is important for environmental management. Sites of

* Corresponding author.
E-mail addresses: joseph.armstrong@abdn.ac.uk (J.G.T. Armstrong), j.parnell@abdn.ac.uk (J. Parnell), l.a.bullock@soton.ac.uk (L.A. Bullock), a.boyce@suerc.gla.ac.uk (A.J. Boyce), magali.perez@abdn.ac.uk (M. Perez), j.feldmann@abdn.ac.uk (J. Feldmann).

https://doi.org/10.1016/j.apgeochem.2019.104401
Received 17 May 2019; Received in revised form 12 August 2019; Accepted 13 August 2019
Available online 14 August 2019

trace element and semi-metal fixation, specifically Se and Te, may also prove important given their low crustal abundance and increasing economic value for use in emerging technologies, such as photovoltaic cells and high-capacity batteries (Chelvanathan et al., 2010; Eftekhari, 2017; Leite et al., 2017; Morales-Acevedo, 2006; Zhou et al., 2017). Identifying new sites of crustal enrichment for these elements is key in targeted exploration and securing adequate future supply of critical metals.

Under anoxic depositional conditions, reduction of chemical compounds causes elemental solubilities to change, resulting in the incorporation of redox sensitive elements within anoxic sedimentary deposits. The most common example of this is sedimentary pyrite mineralisation (FeS_2), where the reaction of detrital Fe^{3+} with bacterially reduced sulphide (S^{2-}) results in pyrite formation in anoxic sediments during deposition and early diagenesis (Raiswell and Canfield, 1998). The majority of trace elements hosted within carbonaceous sedimentary deposits are either incorporated within pyrite or adsorbed onto preserved organic matter (Chappaz et al., 2014; Large et al., 2019; Stüeken et al., 2015b), therefore fluctuations in total organic carbon (TOC) or pyrite abundance can affect trace element concentrations. During deep marine black shale deposition, the fixation of trace elements is dependent on the degree of water anoxia and the concentration of trace elements in the global oceans, which has fluctuated throughout geological time (Large et al., 2019, 2015; Swanner et al., 2014). As such, the two key factors influencing redox sensitive element deposition in carbonaceous sediments are depositional environment and timing.

Elevated trace element concentrations in soils and groundwaters are commonly associated with shale occurrences globally, particularly where lithologies are rich in pyrite and/or organic carbon (Paikaray, 2012; Tabelin et al., 2018). Environmentally hazardous levels of As, Se, lead (Pb) and other elements have been found in drinking waters and soils in China, India, USA and France, primarily sourced from enriched shales or organic-rich sediments (Baruah and Khare, 2010; Cary et al., 2014; Huyen et al., 2019; Islam et al., 2000; Paikaray, 2012; Peters and Burkert, 2008; Zheng et al., 1999). The environmental hazards posed by surface weathering and leaching vary depending on elemental concentrations within individual shale units, as well as the climatic and groundwater conditions in each region (Tuttle et al., 2014a). Leaching and contamination by shales is often enhanced through human activities which increase erosion and surface area, including construction, mining and intensive farming (He et al., 2002; Tabelin et al., 2014; Tuttle et al., 2014b). Understanding common factors controlling trace element accumulation and release in shales is vital for environmental management strategies globally.

Carboniferous (Namurian) black shales of the Bowland Shale formation, North England are known to contain higher than average concentrations of the trace elements Mo, As and Se (Parnell et al., 2018, 2016). Due to the high TOC content and lateral extent of the Bowland Shale, the sequence is considered a prospective shale gas target in the UK (Andrews, 2013; Yang et al., 2016). The lateral equivalent of the Bowland Shale in Ireland, the Clare Shale, has also been discussed for its potential as a shale gas prospect (Jones, 2012; Martinsen et al., 2017) with a comparably high TOC. Extensive outcrops of the Clare Shale and associated secondary mineralisation on the west coast of Ireland provide an ideal study area for assessing the mobility of trace elements within black shale units of equivalent age and depositional setting. This is important for the identification of environmental hazards and economic potential associated with black shales here, and in similar deposits globally. For example, As and Se groundwater mobilisation from the Mississippian Barnett Shale, Texas (Fontenot et al., 2013); Se leaching from the Cretaceous Mancos Shales, Colorado (Tuttle et al., 2014a); As, Mo and U enriched soils from weathering of Precambrian Okchon Gp black shales, Korea (Lee et al., 1998).

Secondary mineralisation associated with the Clare Shales of Western Ireland are used here as a case study for the mobilisation and fixation of trace elements by groundwater. This is an appropriate surface analogue for assessing the mobilisation and fixation potential of trace elements in the subsurface during and after induced hydraulic fracturing for unconventional hydrocarbon extraction. The objectives of this study are as follows:

1. Assess the trace element concentrations of the Carboniferous shales of Western Ireland and their mobility at surface through geochemical and petrographic analysis of in-situ bedrock and weathering deposits.
2. Assess the processes controlling fixation of trace elements during black shale deposition and the formation of oxidised surface deposits, focussing on enriched mineral phases.
3. Identify and discuss any wider environmental implications of this study in relation to trace element mobility during induced hydraulic fracturing of black shales and acid mine drainage remediation.

2. Geological setting

The Carboniferous (Namurian) Clare Shale Formation (Shannon Group) consists of finely laminated, pyritic, deep marine black shales, deposited 326.5–318.5 Ma (Menning et al., 2006; Wignall and Best, 2000). The black shale sequence is up to 180 m thick at surface, (Tanner et al., 2011), with a maximum observed thickness of 280 m in the 'Doonbeg No 1' drill hole, Co Clare (Goodhue and Clayton, 1999). The Clare Shales are underlain by Visean limestones and laterally transition into the overlying, sand-dominated turbidite sequence of the Ross Formation, both of which act as productive aquifers in the region (Gallazzi, 2012) (Fig. 1). The Clare Shale outcrops on the west coast of Ireland, with sections readily accessible at Inishcorker (Co. Clare),

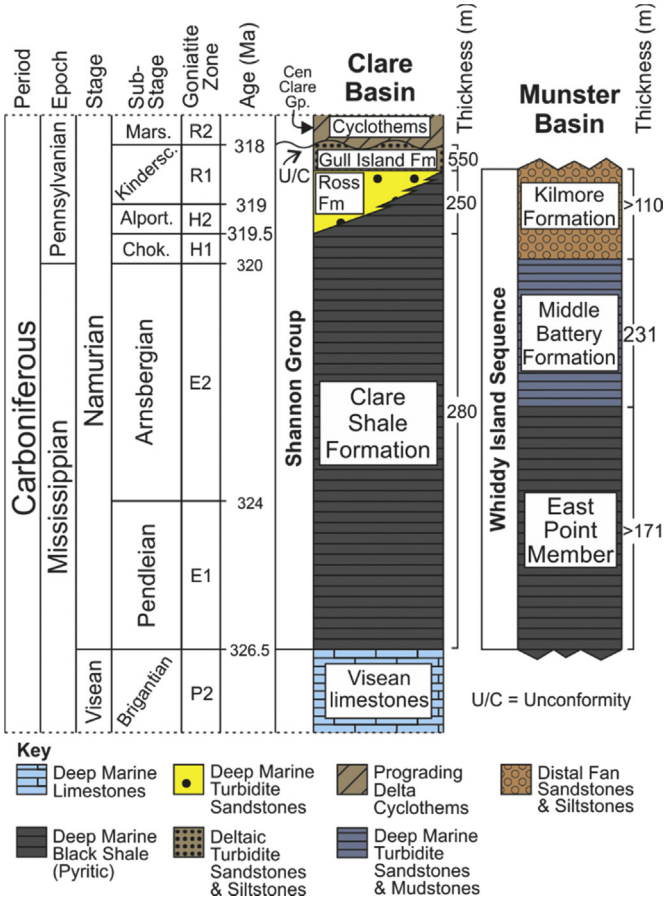

Fig. 1. Stratigraphic log of West Ireland Namurian strata. After Collinson et al., 1991; Goodhue and Clayton (1999); Jones and Naylor (2003); Nolan (2012); Rider (1974); Tanner et al. (2011); Wignall and Best (2000).

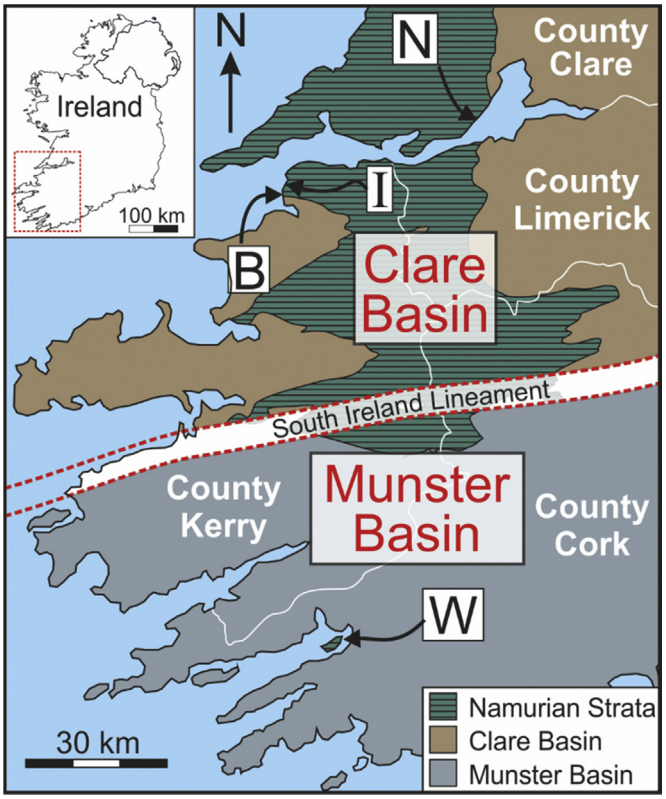

Fig. 2. Sample location map of SW Ireland. Locations of Munster and Clare Basins and distribution of Namurian strata shown. After Gardiner and MacCarthy, 1981; Williams (2000). Sample locations; I = Inishcorker; N = Nun's Beach; B = Ballybunion; W = Whiddy Island.

Ballybunion and Nun's Beach (Co. Kerry). Further south, in the neighbouring Munster Basin, laterally equivalent and comparable Namurian pyritic black shales of the East Point Formation outcrop at Whiddy Island (Co. Cork). (Fig. 2).

At these four localities, groundwater seeps within coastal cliffs of black shale coincide with the occurrence of modern orange-yellow iron-oxide mineralisation on the surface of the black shales (Fig. 3). This mineralisation is up to 30 mm thick, exhibiting textures and geometries indicative of mineral precipitation from solution, rather than *in situ* weathering of the underlying shale, which may form a minor component of these deposits. Previous studies have shown the potential for oxidised ochres to become enriched in trace elements that are mobilised from weathering shale bedrock, particularly in the case of acid mine drainage (AMD) (Bullock et al., 2017, 2018; Parnell et al., 2018).

3. Methodology

3.1. Sampling and preparation

Samples of unweathered Carboniferous black shale and associated precipitates (Fig. 3) were taken from four localities on the west coast of Ireland; Ballybunion Bay, Nun's Beach, Inishcorker Island and Whiddy Island (Fig. 2). Samples of secondary mineralisation were dried in an oven at 50 °C for 24 h. Representative pieces of shale and secondary mineralisation were crushed using a tungsten tema mill until finely powdered (< 64 μm) for bulk geochemical analysis.

3.2. Trace geochemical analysis

Samples of black shale and precipitate were analysed for their bulk elemental composition by method ME-MS41 at ALS Laboratories, Loughrea. 0.5 g of powdered sample was partially digested on a heating block in a solution of aqua regia. The solute was subsequently neutralised and diluted to the required concentration using deionised water before being analysed for elemental abundances by inductively coupled plasma-atomic emission spectroscopy (ICP-AES) and inductively coupled plasma-mass spectroscopy (ICP-MS). Inter-elemental interferences were accounted for in the analysis. This method does not fully dissolve silica phases within samples and should not be considered a whole rock digest, but represents full dissolution of all other mineral phases. This method is highly effective for the analysis of organic and diagenetic mineral components, whilst removing any trace element enrichment effect by detrital silicate input (Xu et al., 2012).

3.3. Major element analysis

Major elemental analysis was performed on samples of secondary mineralisation at ALS Laboratories, Loughrea using ALS fusion disk XRF analysis method ME-XRF26. 0.66 g of crushed sample was fused using a platinum mould into an XRF fusion disk, using a 12 : 22 lithium metaborate: lithium tetraborate flux, with a lithium nitrate oxidizing agent. The disk was then analysed by XRF spectroscopy and total concentrations for major elemental oxides were determined for each sample in conjunction with loss-on-ignition analysis at 1000 °C. Analytical accuracy was ensured by analysis and calibration using blanks and certified standards 629–1 (EURONORM-ZRM), GIOP-102 (Geostats PTY Ltd), SARM-32 (MINTEK), SY-4 (CCRMP).

3.4. Total organic carbon (TOC) and total sulphur (TS)

The total organic carbon (TOC) and total sulphur (TS) contents of the powdered samples were determined using a LECO CS744 at the University of Aberdeen. Total carbon (TC) and TS concentrations were identified by combustion analysis of 0.1 mg powdered sample, using an excess of tungsten and iron chip combustion accelerators. To determine TOC, inorganic carbon was removed by dissolving 0.2 mg of sample in an excess of 20% hydrochloric acid (HCl), producing a decarbonated sample fraction. Decarbonated samples were subsequently analysed for TOC using LECO combustion analysis.

Certified LECO standards were used to produce a multi-point calibration daily before sample analysis. Background C and S contents were accounted for using blanks and subtracted from final values. Each sample was analysed in duplicate and an average calculated to account for any analytical variability. Real standard deviation (RSD) values were calculated for each sample to ensure analytical precision. Where RSD values exceed 5%, samples were reanalysed in duplicate.

3.5. X-ray diffraction (XRD)

Powdered samples were analysed for their bulk mineralogy using XRD analysis. Samples were analysed at room temperature using a PANalytical Empyrean diffractometer using a Cu Kα1 source ($\lambda = 1.54059$ Å). Diffraction patterns were recorded between $5 < 2\theta < 80^{\circ}$ with a step size of 0.013°.

3.6. Sulphur (S) isotope analysis

S-isotope analysis was conducted at the stable isotopes facility at SUERC, East Kilbride, using standard extraction and analysis methods (Robinson and Kusakabe, 1975). Bulk powders of crushed precipitate and pyrite extracted from black shale samples were analysed for their S-isotopic composition. 5–10 mg of each sample was heated to 1100 °C in a vacuum line with an excess of copper(I) oxide (Cu_2O) to convert all available S in the sample to SO_2. Using condensation and pentane traps, the SO_2 gas fraction was isolated from all other extraneous gas phases (N_2 and CO_2). The SO_2 fraction was subsequently analysed for ^{34}S and ^{32}S concentrations using a VG Isotech SIRA II mass spectrometer. The mass spectrometer was calibrated using four reference standards

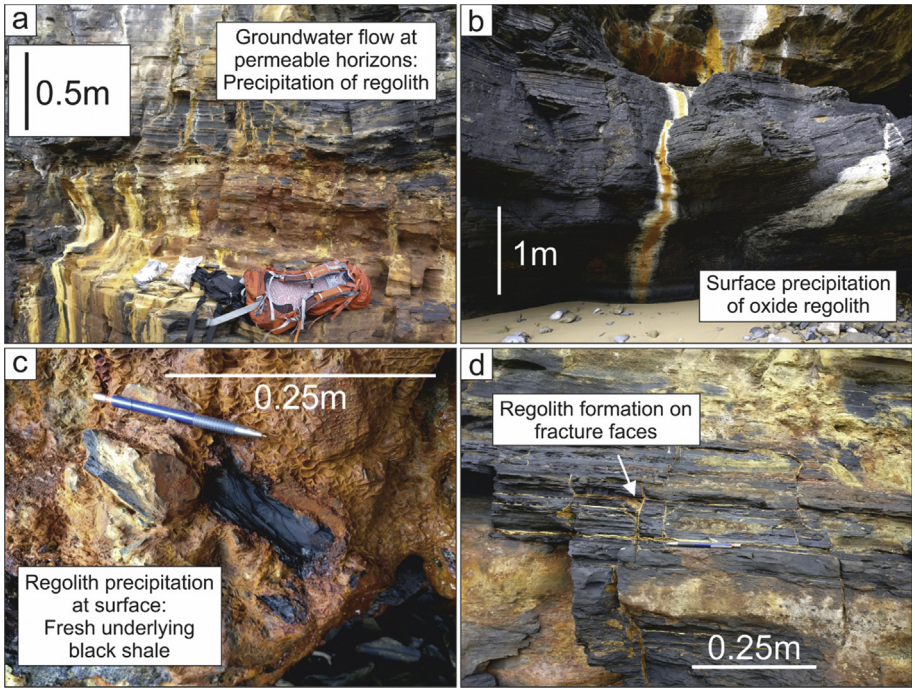

Fig. 3. Examples of secondary oxide precipitation on surface of western Irish black shales: (a) Illustrating precipitation at permeable layers; (b) Surface flow and precipitation of Fe-oxides; (c) Oxide precipitation at surface with unweathered underlying shale; (d) Secondary mineral formation on fracture surfaces.

composing sulphides and sulphates; SUERC internal standards CP-1 and BIS; international reference standards NBS-123 and IAEA-S-3 – with a reproducibility of < 0.2‰ for each standard. The $\delta^{34}S$ for each sample was calculated relative to the Vienna-Canyon Diablo Troilite (VCDT) reference using standard corrections.

3.7. Field emission gun-scanning electron microscopy (FEG-SEM)

High-resolution image analysis was performed at the University of Aberdeen ACEMAC Facility using a Zeiss Gemini field emission gun-scanning electron microscope (FEG-SEM) on polished blocks of black shale and secondary oxide mineralisation. Samples were carbon coated and analysed at 20 Kv, with a working distance of 10.5 mm. Samples were analysed using Oxford Instruments EDS x-ray analysis to assess their mineralogy and any trace element enrichments of > 1%. Unpolished samples of secondary mineralisation were analysed using secondary electron analysis to image growth textures.

3.8. Laser ablation inductively coupled plasma-mass spectrometry (LA-ICP-MS)

Trace element distributions across sample surfaces were analysed using spatially resolved laser ablation inductively coupled plasma-mass spectrometry (LA-ICP-MS) at the University of Aberdeen Trace Element Speciation Laboratory. Cut sample surfaces were prepared by flattening and polishing using carborundum and alumina polishing compounds. Analysis was performed using a New Wave laser ablation system UP213 nm using an output of 1 J cm^2, 10 Hz repetition rate and linked with an Agilent 7900 mass spectrometer. Ablation was performed in a grid-pattern across the sample surface with a round ablation spot size of 100 μm, a line spacing of 100 μm and a 50 μm s^{-1} ablation speed. A 15 s warm-up was applied before ablation start and a 15 s delay was applied between each ablation line. The following isotopes were monitored (dwell time): ^{57}Fe (0.001 s), ^{65}Cu (0.001 s), ^{75}As (0.05 s), ^{78}Se (0.1 s), ^{82}Se (0.1 s), ^{125}Te (0.1 s), ^{126}Te (0.1 s). Parameters were optimised using NIST Glass 612, to obtain maximum sensitivity and to ensure low oxide formation. The ratio $^{232}Th^{16}O+/^{232}Th+$ (as 248/232) was used to assess oxide formation and maintained under 0.3%. A reaction cell was utilised to remove selenium analysis interferences using hydrogen gas. The international sulphide standard MASS-1 (USGS, Reston, VA) was used for quantitative sample calibration prior to analysis. See supplementary data for detection limits and analytical uncertainties.

Element concentration maps were produced using SigmaPlot for Fe, Cu, As, Se and Te in pyritic black shale samples, illustrating the quantitative concentration variations across sample surfaces.

4. Results

4.1. Bulk geochemistry

Bulk analytical results for black shales and secondary mineralisation are summarised in Table 1. See supplementary information for comprehensive geochemical results, detection limits and analytical uncertainties. Average shale and upper crustal concentrations for the elements are given, with ratios calculated for Irish Carboniferous Shale/Average Shale and Regolith/Upper Crustal Average. Average concentrations of cadmium (Cd) (1.99 ppm), cobalt (Co) (158 ppm), Mo (59.3 ppm) and Se (31.6 ppm) for the Carboniferous shales are substantially higher (> 10 times) than average shale values. Average concentrations of As (24.5 ppm), Cu (137 ppm), Te (0.19 ppm) and U (9.52 ppm) are > 2 times higher in Carboniferous shales than average shale values. Average TOC concentrations for the black shales range from 2.87 to 8.05%

The dominant major oxide phases composing the secondary mineralisation are Fe_2O_3 (40.9%), SiO_2 (23.7%), SO_3 (15.6%) and P_2O_5 (4.2%), though proportions of these phases vary between sample sites. There are significant differences in trace element concentrations between the underlying parent shales and the surface oxide mineralisation. Average As concentration (218.1 ppm) is 9 times higher in the secondary mineralisation than the parent shales but is highly variable between sample sites (65.9–447.7 ppm). Average Cu (534 ppm), chromium (Cr) (57 ppm), U (42.9 ppm), and vanadium (V) (397 ppm) are 4–6 times higher than those in the average parent shale. Average concentrations of Se (60.1 ppm) and thorium (Th) (8.5 ppm) are 2 times

Table 1
Summary bulk analysis data for shale and regolith (secondary mineralisation) samples. *Average upper crust and average shale values given for comparison (Hu and Gao, 2008; Rudnick and Gao, 2003; Stüeken et al., 2015a).*

Locality	Lithology	No. of Samples	TOC (%)	As (ppm)	CaO (%)	Cd (ppm)	Cu (ppm)	Co (ppm)	Cr (ppm)	Fe (%)	Fe_2O_3	Mo (ppm)	Ni (ppm)	Pb (ppm)
Analytical Method			LECO	ME-MS41	ME-XRF26	ME-MS41	ME-MS41	ME-MS41	ME-MS41	ME-MS41	ME-XRF26	ME-MS41	ME-MS41	ME-MS41
Ballybunion Bay	Shale	6	6.55	15.5	–	1.02	114	96	9	2.04	–	125.2	34.2	17.8
	Regolith	5	0.31	85.4	0.4	0.47	821	14	67	25.46	38.47	73.5	14.3	15.7
Nun's Beach	Shale	4	3.22	14.9	–	5.16	109	45	9	1.75	–	11.0	46.3	20.8
	Regolith	4	0.34	249.8	1.2	0.36	268	38	55	24.25	39.05	85.5	37.1	15.5
Inishcorker	Shale	4	2.87	12.6	–	0.83	106	33	30	8.26	–	10.0	70.2	14.7
	Regolith	3	1.16	447.7	0.2	6.86	494	45	29	30.07	46.54	61.1	177.8	26.5
Whiddy Island	Shale	3	8.05	71.0	–	1.27	266	598	20	8.86	–	57.7	132.2	46.0
	Regolith	1	2.31	65.9	0.2	0.15	290	40	105	27.80	43.85	65.2	29.5	9.4
Average Carboniferous Shale		17	5.16	24.5	–	1.99	137	158	16	4.64	–	59.3	62.8	22.7
Average Regolith		13	0.67	218.1	0.6	1.88	534	31	57	26.33	40.92	73.7	60.2	17.6
Average Shale			–	**8.6**	**-**	**0.05**	**36**	**16**	**85**	**4.38**	**-**	**1.2**	**35.9**	**19.5**
Upper Crustal Average			–	**5.7**	**3.6**	**0.06**	**27**	**15**	**92**	**3.91**	**5.04**	**0.6**	**34.0**	**17.0**
Carboniferous Shale/Average Shale			-	***2.8***	**-**	***39.9***	***3.8***	***10.1***	***0.2***	***1.1***	**-**	***48.6***	***1.7***	***1.2***
Regolith/Upper Crust			-	***38.3***	***0.2***	***31.4***	***19.8***	***2.0***	***0.6***	***6.7***	***8.1***	***122.8***	***1.8***	***1.0***

Locality	**Lithology**	**No. of Samples**	**P (ppm)**	**P_2O_5 (%)**	**Re (ppm)**	**S (%)**	**SO_3 (%)**	**Se (ppm)**	**SiO_2**	**Te (ppm)**	**Th (ppm)**	**Tl (ppm)**	**U (ppm)**	**V (ppm)**
Analytical Method			**ME-MS41**	**ME-XRF26**	**ME-MS41**	**LECO**	**ME-XRF26**	**ME-MS41**	**ME-XRF26**	**ME-MS41**	**ME-MS41**	**ME-MS41**	**ME-MS41**	**ME-MS41**
Ballybunion Bay	Shale	6	205	–	0.208	0.53	–	29.5	–	0.16	2.6	0.26	6.78	67
	Regolith	5	3730	0.91	0.003	9.80	26.92	23.5	10.5	0.22	3.4	12.10	11.87	675
Nun's Beach	Shale	4	573	–	0.043	2.11	–	20.3	–	0.16	6.1	0.22	14.41	37
	Regolith	4	10000	7.67	0.008	4.33	12.50	114.0	18.5	0.19	16.2	0.99	94.03	277
Inishcorker	Shale	4	2350	–	0.058	2.63	–	10.8	–	0.10	4.0	0.24	8.68	98
	Regolith	3	10000	5.91	0.030	1.32	3.81	59.7	20.0	0.09	7.6	0.53	36.97	175
Whiddy Island	Shale	3	2943	–	0.200	8.78	–	78.8	–	0.43	3.0	0.11	9.61	52
	Regolith	1	5420	1.42	0.019	2.46	7.31	29.0	29.0	0.24	6.4	0.10	11.45	148
Average Carboniferous Shale		17	1279	–	0.132	2.85	–	31.6	–	0.19	3.8	0.22	9.52	64
Average Regolith		13	7236	4.18	0.012	5.60	15.64	60.1	23.7	0.18	8.5	5.09	42.91	397
Average Shale			**698**	**0.16**	**Varies**	**Varies**	**-**	**1.3**	**-**	**0.05**	**18.0**	**1.08**	**3.56**	**112**
Upper Crustal Average			**654**	**0.15**	**0.0002**	**0.06**	**0.16**	**0.1**	**66.6**	**0.03**	**10.5**	**0.55**	**2.60**	**97**
Carboniferous Shale/Average Shale			***1.8***	**-**	**-**	**-**	**-**	***24.3***	**-**	***3.8***	***0.2***	***0.2***	***2.7***	***0.6***
Regolith/Upper Crust			***11.1***	***27.9***	***59.6***	***93.3***	***97.8***	***667.9***	***0.4***	***6.8***	***0.8***	***9.2***	***16.5***	***4.1***

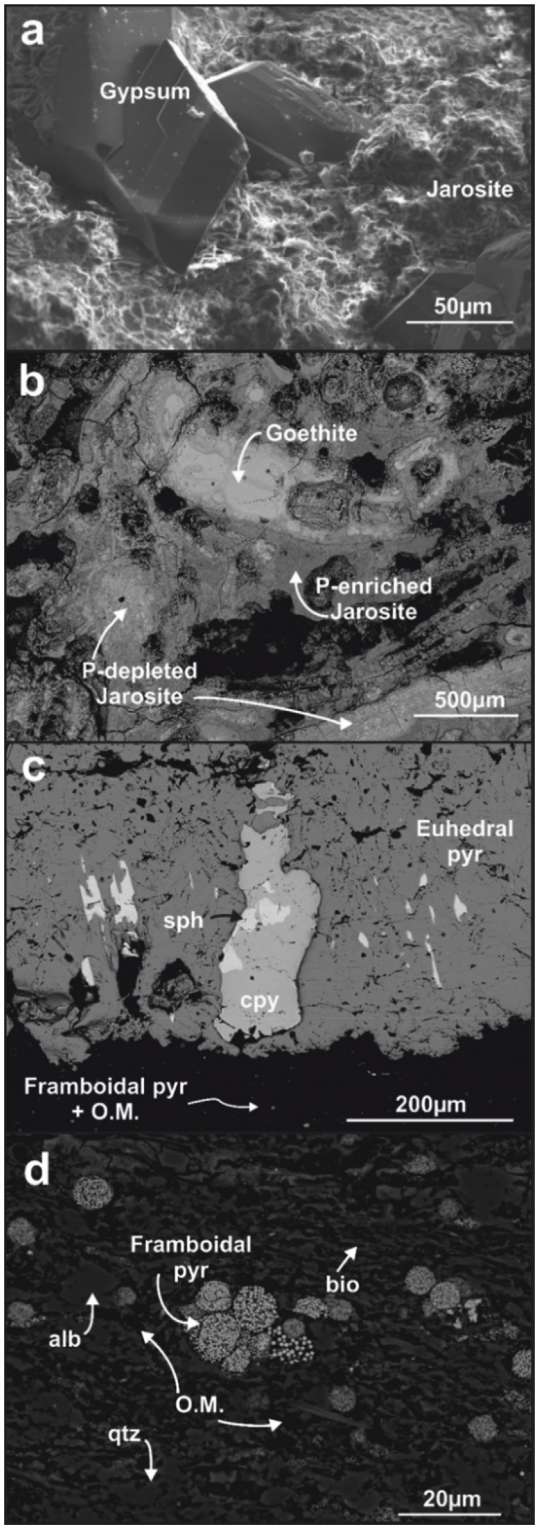

Fig. 4. SEM imagery of Nun's Beach secondary mineralisation (a & b) and Whiddy Island pyritic black shales (c & d): (a) Secondary SEM image of unpolished secondary mineralisation, illustrating growth textures of gypsum and jarosite; (b) Backscatter SEM image of polished secondary mineralisation, illustrating layered oxide mineralisation of geothite and jarosite. Phosphate (P)-enriched jarosite appears less bright due to lower average atomic number; (c) Backscatter SEM image, illustrating extensive pyrite (pyr) mineralisation, with minor sphalerite (sph) and chalcopyrite (cpy); (d) Backscatter SEM image, illustrating small scale (mud grade) framboidal pyrite, organic matter (O.M.), biotite (bio), quartz (qtz) and albite (alb).

higher than those in the parent shale, though Se concentrations are highly variable (23.5–114.0 ppm). The average thallium (Tl) concentration (5.09 ppm) of the oxidised deposits is 9 times higher than in the upper crust and > 20 times the Carboniferous shales, though this is due to anomalously high concentrations of Tl at Ballybunion. Other Irish sampling localities do not show comparable enrichments of Tl relative to the parent shales. Other trace element and base metal concentrations (Cd, Mo, Ni, Pb and Te) are similar in concentration or less than that in the parent shales. TOC concentrations within the secondary mineralisation average 0.67%, which is approx. 10% of that found in the parent shales, though values range 0.22–2.31% in all samples.

4.2. Sample mineralogy

SEM analysis of the Clare Shale shows that samples are abundant in pyrite and organic matter, with discrete phases of chalcopyrite ($CuFeS_2$) and sphalerite ((Zn,Fe)S) present within the pyrite (Fig. 4c). The composition of quartz, albite, muscovite, biotite, chlorite and pyrite (framboidal and euhedral) is typical of a standard deep marine shale (Fig. 4d). No other discrete trace element mineralisation was identified.

XRD analyses of the secondary mineralisation indicate that the dominant mineral phases in all analysed samples are goethite (FeO(OH)), jarosite ($(H_3O)Fe_3(SO_4)_2(OH)_6$) and quartz (SiO_2), with minor amounts of gypsum ($CaSO_4.2H_2O$). Mineral d-spacing values identified; goethite (3.4 Å, 2.7 Å); quartz (3.3 Å, 1.8 Å, 2.3 Å); jarosite (2.3 Å, 3.1 Å, 5.1 Å, 2.0 Å, 1.8 Å); gypsum (7.6 Å). See supplementary data for labelled XRD spectra.

SEM backscatter and EDS analysis of these deposits identified variable concentrations of phosphorus (P) within jarosite mineralisation (Fig. 4). No other P-bearing mineral phases were detected within the secondary mineralisation. The major mineral phases identified were detrital quartz, Fe-oxide (goethite) and jarosite, which coincides with XRD analysis. Minor gypsum mineralisation was also identified. Secondary SEM imagery of unpolished samples shows three-dimensional mineral growth textures (Fig. 4a). Discrete layering of oxide mineral phases is evident in backscatter imagery (Fig. 4b).

4.3. S-isotope analysis

The sulphur isotopic compositions ($\delta^{34}S$) of the pyrite within sampled shales and the associated secondary sulphate (jarosite) deposits are given relative to the VCDT standard (Fig. 5). All shale pyrite values are negative, while the corresponding jarosite mineralisation has a consistently lighter sulphur isotope ratio than the parent shale pyrite. $\delta^{34}S$ values for other potential sources of artificial and natural sulphate are shown. The $\delta^{34}S$ ratio for Namurian seawater sulphate was approximately 15.8‰ (Kampschulte and Strauss, 2004).

4.4. LA-ICP-MS analysis

Laser ablation maps (Fig. 6a & b) of the Carboniferous shales show the trace element enrichment zones for Se and As. Sulphide mineralisation is indicated by areas of increased iron (Fe) concentration. Se, Cu and As enrichments are closely associated with sulphide mineralisation in all samples, though Cu enrichment is inconsistent between sulphides. Te enrichment is not associated with the sulphide mineralisation and is distributed as discrete inclusions < 100 μm throughout sample matrix.

5. Discussion

5.1. Carboniferous black shales

5.1.1. Elemental enrichments

Bulk elemental analysis (ICP-AES & ICP-MS) shows higher trace element abundances in the Carboniferous shales compared to both

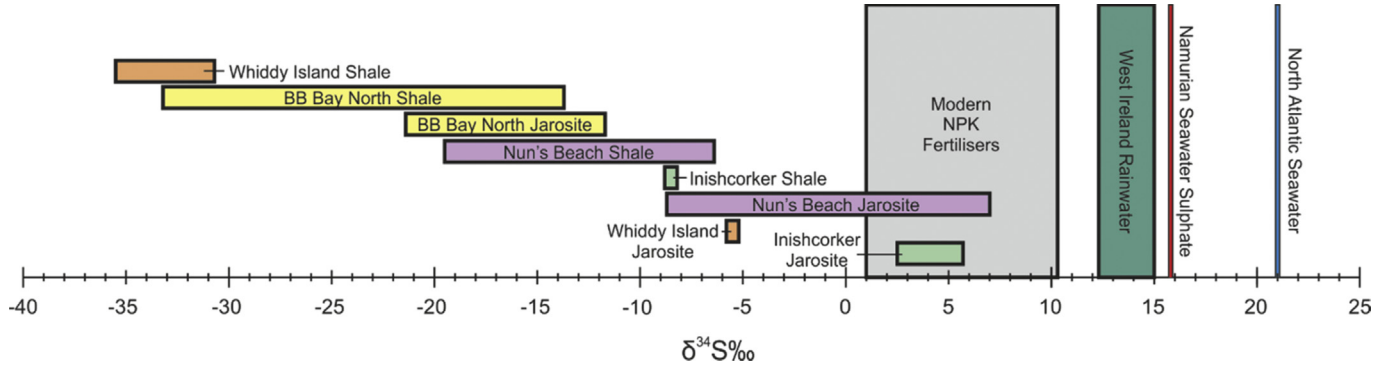

Fig. 5. ***Sulphur isotope data for Irish shale pyrite and jarosite samples****. Reference values given for modern artificial fertilisers (Moncaster et al., 2000), west Ireland rainwater (Novak et al., 2001), North Atlantic seawater (Böttcher et al., 2007) and Namurian seawater (Kampschulte and Strauss, 2004).*

average crustal and average shale values (Table 1). Concentrations up to 10 times higher than average shale are observed for As, Cu, Ni, Te and U. Concentrations > 10 times higher than average shale are observed for Cd, Co, Mo and Se. Trace element abundances for As, Se and Mo are comparable to those in the laterally equivalent Bowland Shale, Northern England (Parnell et al., 2016), though all are slightly elevated in the Irish shales. For example, average Se and As in the Bowland shale are 21.1 and 22.8 ppm respectively, whilst in the Irish shales they are 31.6 and 24.5 ppm respectively.

LA-ICP-MS analysis maps (Fig. 6a and b) show homogenously elevated concentrations of the redox sensitive trace elements Se and As are present within pyrite in the Carboniferous black shales, indicating anoxic conditions during deposition or early diagenesis. Discrete mineral phases of chalcopyrite within bedding parallel pyrite (Fig. 4c) account for the high Cu abundance in the black shales, which are also indicative of anoxic, metalliferous depositional conditions (Calvert and Pedersen, 1993). Minor Te enrichments distributed throughout the sample matrix is most likely associated with adsorption onto organic matter or mineralisation within microscopic pyrite crystals (Armstrong et al., 2018). Average Re/Mo, V/Cr and U/Th ratios of 2.8 (ppb/ppm), 4.2 (ppm/ppm) and 2.5 (ppm/ppm) respectively and average TOC and TS values of 5.16% and 2.85% respectively are indicative of suboxic-anoxic deep marine deposition for these sedimentary deposits (Crusius et al., 1996; Jones and Manning, 1994). An average Mo concentration of 59.3 ppm also indicates intermittent euxinic conditions (Scott and Lyons, 2012).

Isotopically light $\delta^{34}S$ values for the black shale pyrite samples, ranging from −35.5 to −8.2‰ (Fig. 5) demonstrate substantial isotopic fractionation from the Namurian seawater sulphate average of 15.8‰ (Kampschulte and Strauss, 2004). This is indicative of pyrite formation through bacterial sulphate reduction under anoxic depositional conditions (Hall et al., 1994). The trace elements Cd, Co, Mo, Ni and U are all commonly elevated in black shales due to deposition under anoxic conditions (Rimstidt et al., 2017), though the extent of trace element enrichment has varied through geological time (Large et al., 2019).

5.1.2. *Implications for black shale deposition*

The relative crustal enrichments in redox sensitive trace elements, including As, Cd, Cu, Co, Mo, Se, Te and U, in the Irish shales and their lateral equivalents are globally significant as they indicate deposition in a stratified, deep marine basin, which promoted the accumulation of trace elements from waters that were inherently trace element enriched (Large et al., 2019). This increase in elemental availability in deep marine settings during the Carboniferous is either indicative of higher trace element concentrations in global marine basins at that time (Large et al., 2017, 2014), or at least higher trace element concentrations in isolated deep marine settings (Canfield et al., 2008; Stüeken et al., 2015b). An increase in global oceanic trace element abundances during the Carboniferous, specifically Se, has been proposed previously (Large et al., 2019), during which time atmospheric oxygen concentration increased to 20% above present atmospheric levels. Periodic increases

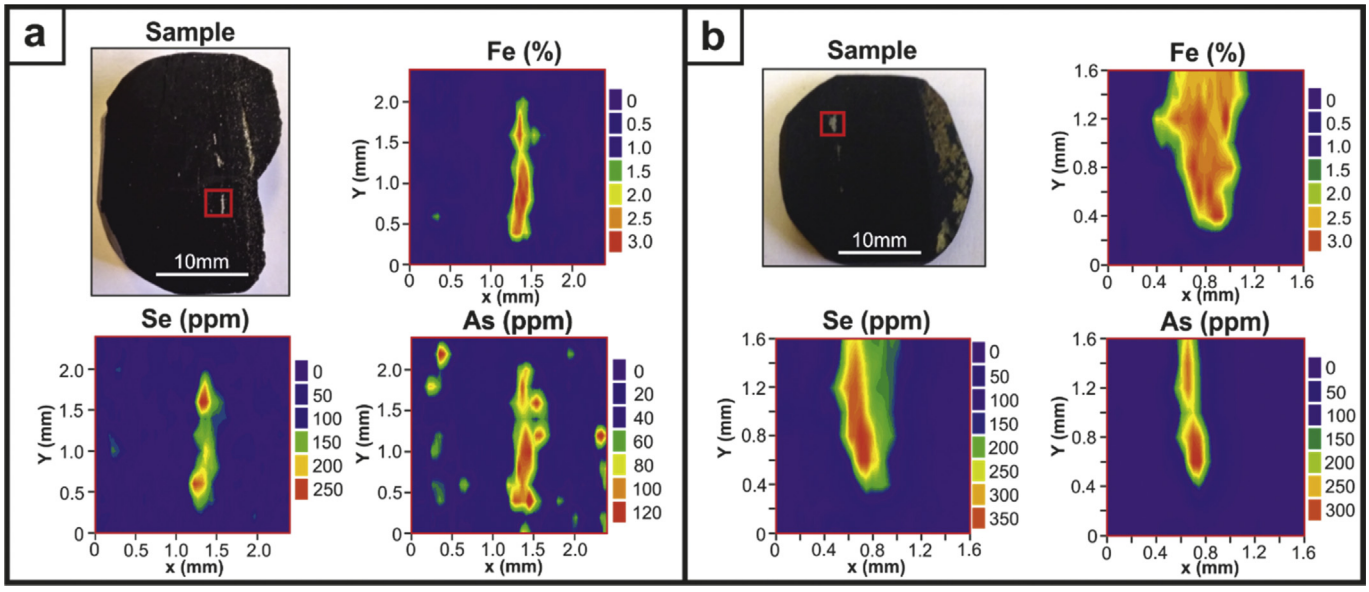

Fig. 6. LA-ICPMS maps for pyritic Carboniferous shale samples. Se and As enrichment within pyrite mineralisation (Fe maps): (a) Whiddy Island; (b) Ballybunion.

in atmospheric O_2 increased continental weathering rates and the flux of trace elements to the oceans (Campbell and Squire, 2010). Increased redox sensitive trace element abundances in deep marine deposits have also been observed during other geological periods when atmospheric O_2 concentrations have increased substantially, such as the late Neoproterozoic (Armstrong et al., 2018).

5.2. Secondary mineralisation

5.2.1. Trace element mobility and fixation

The surficial precipitate deposits at the four sampled sites exhibit mineralogies and trace element abundances substantially different from those of the associated black shales (Table 1; Fig. 4). These deposits, composed of goethite, jarosite, gypsum and detrital quartz, formed by the near-surface oxidation of the pyritic shale, mobilisation of the liberated elements by correspondingly acidic groundwaters and precipitation of oxide minerals at surface under higher pH surface conditions (Fig. 3). Goethite, jarosite and gypsum mineralisation are typical near abandoned mining sites where sulphide weathering and oxidisation produces acid-mine drainage (AMD) consisting of sulphates and Fe-oxides (Acero et al., 2006). Quartz mineralisation found in the secondary mineralisation is likely detrital, from the underlying black shales, as conditions are not appropriate for the dissolution and precipitation of quartz coeval with oxide phases and in SEM, quartz is present in discrete grains, not layers. The trace element abundances within these oxide deposits can be considered in terms of enrichment factor from the parent shale (Fig. 7), where values > 1 indicate enrichment of trace elements, while values < 1 indicate depletion of trace elements. The extent of these enrichments is dependent on several factors, including liberation of trace elements from parent shale, mobility of elements in associated groundwaters, mobility of trace elements under surface pH and oxidation (Eh) conditions, and affinity for fixation within oxide mineralisation.

The liberation of trace elements from the parent shale is predominantly associated with the oxidation of pyrite, as this is the primary site of trace element concentration (Fig. 4; Fig. 6). Pyrite is unstable under oxidising conditions, the breakdown of which results in acid production (H^+), which promotes further chemical weathering and commonly results in the formation of AMD (Sheoran and Sheoran, 2006). Organic matter also becomes unstable under oxidising conditions, the breakdown of which releases any organically bound trace elements (Dang et al., 2002). Many potentially hazardous elements which are present in pyritic carbonaceous lithologies, including Fe, S, Se, As, Cd, Cu and Tl, can become mobilised under low pH, oxidising groundwaters through the breakdown of pyrite and organic matter (Baruah and Khare, 2010; Xiao et al., 2012). At surface, the pH of the emergent acidic groundwaters increases by interaction with meteoric water and sea-spray which reduces the mobility of the dissolved elements and induces precipitation of major oxide phases, including goethite and jarosite, with the potential for incorporation of compatible trace elements (Balistrieri and Chao, 1987; Bullock et al., 2017). In particular, the leaching of Se and As from deep marine sedimentary lithologies and subsequent adsorption onto evaporitic deposits is known to be a pH controlled process (Smedley and Kinniburgh, 2002; Tabelin et al., 2017), with leaching and adsorption onto goethite generally promoted under lower pH conditions (Jacobson and Fan, 2019). Trace element fixation is commonly observed at sites of AMD and utilised as a stage in many remediation strategies where Fe-oxide precipitation is commonly promoted through chemical and bacterial processes (Johnson and Hallberg, 2005). Arsenic fixation during AMD formation of goethite, jarosite and schwertmannite is a well-known and utilised remediation method (Acero et al., 2006; Asta et al., 2009).

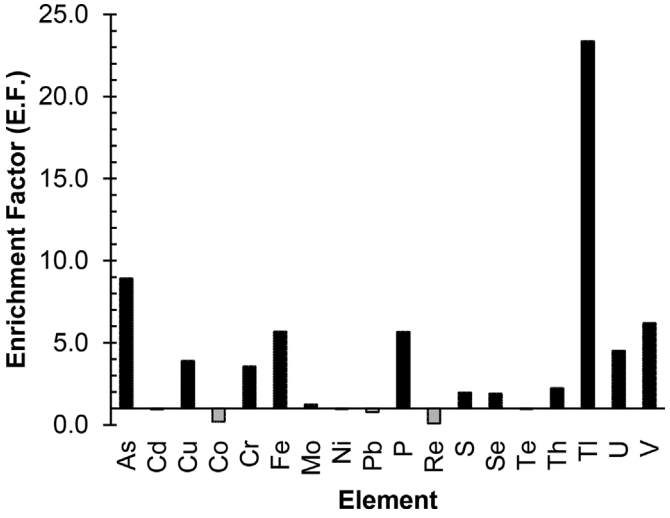

Fig. 7. Elemental enrichment factor (E.F.) data for oxide samples relative to parent shale. E.F. = elemental concentration in oxide/element concentration in associated shale. Values > 1 indicate enrichment within oxides; values < 1 indicate depletion.

Compared to average upper crustal values, the following elements are enriched in the secondary oxide mineralisation (Table 1); Se (668x), Mo (123x), As (38x), Cd (31x), Cu (20x), U (16.5x), Tl (9.2x), Te (6.8x), V (4.1x), Co (2x), Ni (1.8x). This indicates partial adsorption of these elements onto the oxide phases after leaching, though many of these enrichments reflect high concentrations from the parent shales. Chromium, Pb and Th are not enriched relative to average crust, indicating limited adsorption to Fe-oxides and/or reduced solubility of these elements in the groundwater. This could suggest limited leaching from parent shales, or precipitation of Cr, Pb and Th phases prior to Fe-oxide, due their lower solubility.

Of those elements that are elevated compared to upper crust, As, Cu, U, V, Se, Tl all have enrichment factors > 1 when compared to the parent shales (Fig. 7). This indicates preferential leaching of these elements from the parent shales and fixation onto oxide phases. Arsenic, Cu and Se are predominantly leached through the oxidation of pyrite in the shales (Fig. 6), while U and V are most likely sourced through oxidation of organic matter (Breit and Wanty, 1991; Luning and Kolonic, 2003). Thallium may have been sourced from pyrite or organic matter breakdown (Lipinski et al., 2003).

An important consideration when identifying elemental enrichments in secondary mineralisation compared to parent shales is the relative depletion of trace elements which may have occurred in the shale formations during surface weathering processes. Considering the exposed locations of the sampling sites and the active leaching of trace elements from the shales, it is possible that the sampled formations are depleted in comparison to their original depositional values. As such, the enrichment factors observed in the secondary mineralisation may be higher than if they were compared to unexposed shale samples at depth. To mitigate this effect, only samples of the least weathered shales were taken for analysis, with sites of active weathering or leaching avoided during sample collection. Where possible, samples were taken from sheltered areas or taken from depth within cliff faces. While this should limit the observed surface weathering of the sampled shale formations, minor depletion of trace elements from the parent shales can not be discounted. The higher than average trace element concentrations observed in the parent shales, specifically those resident in within unstable mineral phases of pyrite (As, Cu, Se) and O.M. (Te, U), suggests that depletion of trace elements was not significant for the samples analysed.

5.2.2. Phosphate substitution within jarosite

Previous studies on mineralisation at Ballybunion have identified numerous occurrences of secondary phosphate and sulphate mineralisation (Francis and Ryback, 1987; Moreton et al., 1995; Rumsey, 2016) associated with the black shales at surface, some of which are

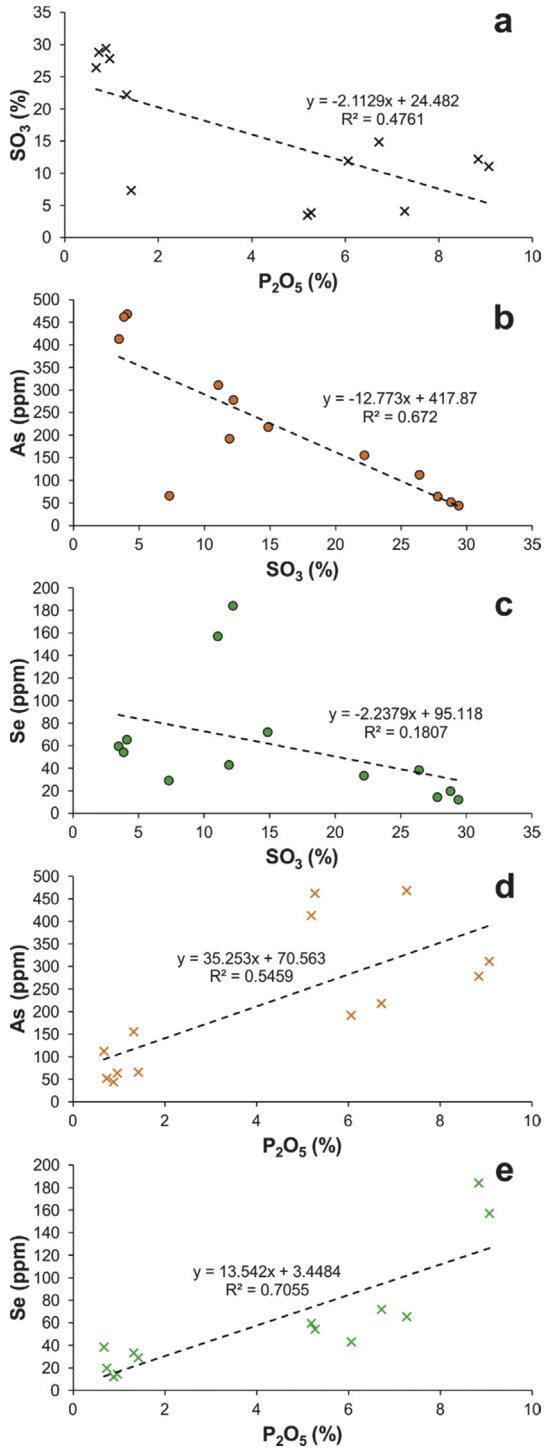

Fig. 8. Geochemical cross-plots for oxide samples: (a) Phosphate (P_2O_5) vs sulphate (SO_3). Inverse relationship between P_2O_5 and SO_3; (b) SO_3 vs As; (c) SO_3 vs Se; (d) P_2O_5 vs As; (e) P_2O_5 vs Se. Variations in SO_3 and P_2O_5 concentrations broadly correlate with those of As and Se.

unique in the British Isles. Bulk geochemical analysis of the secondary mineralisation at all sites indicate variable, inversely proportional concentrations of phosphate and sulphate at 0.6%–9.1% and 3.5%–29.4%, respectively (Fig. 8a). XRD analysis indicates that there are no distinct phosphate minerals in abundance within these deposits, despite bulk P_2O_4 concentrations in excess of 9 wt %, while the sulphate mineral jarosite is a primary component of all deposits. SEM EDS analysis indicates the presence of phosphorus within jarosite (Fig. 4b), indicating substitution of phosphorus within the jarosite sulphate structure. Substitution of phosphate anions (PO_4^{3-}) for sulphate (SO_4^{2-}) within jarosite has been demonstrated under laboratory conditions in other studies, given the similarity in the ionic radii of these two ions, indicating a partial solid solution between a purely sulphatic and a phosphatic phase (Dutrizac and Chen, 2010). The inverse relationship between total SO_3 and P_2O_5 concentrations identified in the oxide samples (Fig. 8a) indicates direct substitution of sulphate anions for phosphate within the jarosite structure, though variations in total jarosite content between samples increases the spread of data points. This substitution is here demonstrated under ambient temperature and pressure conditions through precipitation from sulphate and phosphate saturated waters.

S-isotope ($\delta^{34}S$) values ranging -21.4 to $+7.0$‰ for the secondary mineralisation (Fig. 5) indicate that the S in the jarosite is primarily sourced from the isotopically light, bacterially reduced sulphides of the underlying black shales ($\delta^{34}S = -35.5$ to -8.2‰). The wide distribution of $\delta^{34}S$ values from the jarosite samples, which are consistently heavier than the corresponding pyritic shale values, indicates a partial sulphate input from isotopically heavier sources, potentially modern seawater or artificial fertilisers (Fig. 9).

Identification of the phosphate source is more challenging. A significant phosphate source is available from the organo-phosphates within the underlying shales (average 4.18% P_2O_5), though phosphate may also be sourced from modern seawater, artificial fertilisers or meteoric waters. Given the proximity to the coast, groundwaters at all four sampling sites are likely to contain significant concentrations of seawater, suggesting a mixed source for both SO_4 and PO_4.

5.2.3. *Trace element compatibility of oxide phases*

Comparison of the most substantially enriched trace elements within the samples of secondary mineralisation reveals significant variations in their concentration. As (44–468 ppm), Cu (235–1180 ppm) Se (12–184 ppm), Tl (0.1–19.5 ppm) and V (148–847 ppm) concentrations vary by at least an order of magnitude, with no corresponding variation within the underlying parent shales. U concentration (5.86–158 ppm) approximately correlates with variation in the parent shales. When compared to the major oxide concentrations in the secondary mineralisation, increasing concentrations of As and Se correlate with increasing concentrations of P_2O_5 and correspondingly lower SO_3 concentrations (Fig. 8 b-d). This suggests a greater compatibility for oxidised trace element species of As and Se within PO_4-bearing jarosite, or alternatively an increase in trace element mobility in PO_4 enriched groundwaters. There is no observable correlation between As or Se with the major oxide phase Fe_2O_3 in the samples, despite a common association of As and Se with goethite and other Fe-oxides in

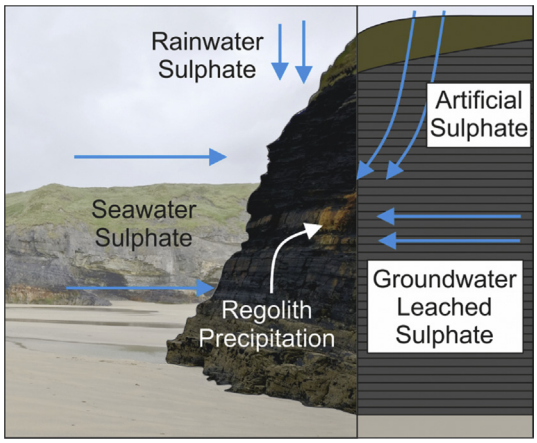

Fig. 9. Diagram of sulphate formation on surface of black shales. Potential sulphate sources are indicated and their transport pathways.

oxidised weathering deposits (Strawn et al., 2002). The observed spread of data points is likely due to minor influencing factors, including the proportion of mineral phases between samples and the availability of As and Se in groundwaters at each sampling site.

Interaction between PO_4^{3-} and selenite (SeO_3^{2-}) has been identified in biological systems, where PO_4^{3-} can have a significant effect on overall Se uptake in plant systems, due to the similar chemical properties of PO_4^{3-} and SeO_3^{2-} (Liu et al., 2018). Under synthetic conditions, phosphate anions have been recognised to have a high affinity for adsorption of As and Se species (Balistrieri and Chao, 1987; Jacobson and Fan, 2019). Furthermore, synthetic laboratory analysis has shown that the anions selenate (SeO_4^{2-}), arsenate (AsO_4^{3-}) and PO_4^{3-} can all substitute for SO_4^{2-} within jarosite, with a complete solid solution occurring with selenate and sulphate end-members (Baron and Palmer, 1996; Dutrizac et al., 1981; Dutrizac and Chen, 2010; Paktunc and Dutrizac, 2003). The results presented here suggest that phosphate substitution within the structure of jarosite in naturally occurring systems increases the ease for further partial substitution of other similarly sized and charged anions, including SeO_4^{2-} and AsO_4^{3-} and others. This preferential substitution of Se and As into phosphatic oxide phases has potential implications for the design of AMD remediation methods (Asta et al., 2009). Where the formation of phosphate-rich jarosite can be induced in AMD waters, improved fixation of potentially toxic trace elements may be achieved. The elevated phosphate contents of most agricultural fertilisers could provide a source of dissolved phosphate in many systems already.

The negative correlation between Fe_2O_3 (goethite) concentration and As or Se concentrations of the these deposits in unusual, considering goethite is commonly recognised as a dominant site for As and Se adsorption during AMD formation (Acero et al., 2006; Jacobson and Fan, 2019). This may relate to the higher pH setting of mineral formation (on sea-cliffs), where adsorption of As and Se onto goethite is less kinetically favourable (Jacobson and Fan, 2019). Additionally, no correlation between the major oxide phases and Cu, Tl or V are observed, indicating that trace element leaching or fixation of these elements are being controlled by other factors, potentially flow-rate or pH.

5.3. Implications for hydraulic fracturing

The Clare Shale and the laterally equivalent Bowland Shale in Northern England have been recognised for their prospectivity as unconventional shale gas resources (Andrews, 2013; Jones, 2012; Martinsen et al., 2017; Yang et al., 2016). Significant public and scientific concern has been expressed for the potential contamination of land and groundwaters around prospective sites of shale gas extraction (Centner, 2013; Fontenot et al., 2013; Gallazzi, 2012; Osborn et al., 2011; Parnell et al., 2016), though conclusive evidence of contamination is generally lacking and often disputed (McHugh et al., 2014). The significant elemental enrichments identified here in the Carboniferous shales and the demonstrated mobility of As, Se, U and other trace elements in natural groundwater could be of environmental concern during and after hydraulic fracturing operations.

The process of induced hydraulic fracturing increases the surface area within hydrocarbon reservoirs at depth in order to increase formation permeability and allow the available hydrocarbons to be extracted more efficiently (Settari, 1980). In the case of unconventional shale gas extraction, this process is applied to very low permeability, organic-rich black shales. A key concern regarding induced hydraulic fracturing is the potential to alter groundwater pathways at depth, leading to the eventual contamination of ecosystems and drinking waters (Fig. 10). Most investigations into groundwater contamination from hydraulic fracturing processes are concerned with contamination from chemical additives or produced hydrocarbons. This research highlights the widely overlooked contamination source of element leaching from the *in situ* black shale bedrock, which is shown in Irish Carboniferous shales to be abundant in many hazardous trace elements, including As, Cd, Se and U. Previous studies have highlighted potential Se and As contamination of drinking waters in regions nearby hydraulic fracturing sites in the Barnett Shales, USA (Fontenot et al., 2013), though the precise source of the contamination could not be identified. Synthetic laboratory investigations on potential leaching rates from the Devonian Marcellus Shale, USA have found that both saline groundwater brines and injected hydraulic fracturing waters have the potential to leach As, Se and barium (Ba) from the formation under elevated temperatures (Balaba and Smart, 2012; Renock et al., 2016). Additionally, deposition of the Barnett Shale, a major shale gas target in the USA, was co-eval with that of the Namurian Irish Shales (Pollastro et al., 2007), suggesting that similar enrichments of hazardous trace elements may occur in this formation.

The elemental enrichments within the Carboniferous black shales of western Ireland and the identified mobilisation of trace elements by associated groundwater make a reasonable analogue for groundwater processes at depth. We suggested that during hydraulic fracturing processes, both nearby groundwater and produced waters could become contaminated through the chemical weathering of black shale formations and subsequent leaching of trace elements. The increased surface area and potential alteration of groundwater pathways after fracturing may result in disruption of the established groundwater equilibrium, as has been observed in mining sites globally (Johnson and Hallberg, 2005).

Due to the significant depth required for adequate organic maturation and hydrocarbon production (> 2 km), it is likely that any groundwaters present near sites of induced fracturing would be in a reduced (low O_2) state (Grenthe et al., 1992), in contrast to the widely oxidative conditions found near-surface. This could prove to be a mitigating factor in the potential leaching of hazardous trace elements from enriched shales at depth, as this would limit the chemical weathering of O.M. and pyrite by oxygen. However, the routine use of acids during the hydraulic fracturing process, for the purpose of formation dissolution and fracturing widening (Guo et al., 2017; Vengosh et al., 2014), have a direct chemical weathering effect on shale formations. Pyrite and O.M. are susceptible to chemical breakdown under acidic conditions (Descostes et al., 2004; Li et al., 2010), which results in a further release of H^+ ions which can contribute to the weathering process (Johnson and Hallberg, 2005). While the chemical breakdown and trace element leaching will be slower in a reducing environment than under surface oxidative conditions, it should still be considered as a potential hazard in artificially fractured formations, particularly where acid-induced fracture propagation is utilised. Additionally, under reducing groundwater conditions, the solubility and leaching rates of As increase significantly (Tabelin et al., 2018), primarily due to the instability of Fe-oxyhydroxide phases which As readily adsorbs to. Cases of dangerously elevated groundwater As concentrations in Bangladesh are associated with highly reducing groundwaters due to increased solubility and limited As adsorption (Zheng et al., 2004). This could therefore result in increased mobility of As and other trace elements leached from enriched shale formations associated with reducing groundwaters, due to the instability of available oxyhydroxide phases, like those observed at surface in Western Ireland.

Given the findings and implications of this study, it is suggested that waters associated with induced hydraulic fracturing are closely monitored for minor trace element contamination, including As, Se, Tl and U. It is possible that significant contamination may not occur until hydrocarbon production ceases and groundwater equilibrium is re-established, similar to that seen in AMD sites after mine flooding (Johnson and Hallberg, 2005). It is however possible that the predominantly reducing conditions present at these depths may limit the oxidation and trace element leaching of shale sequences. Remediation of contaminated land or produced waters would be expensive and may need to be considered during planning stages. However, leaching and extraction of critical trace elements during these processes could provide a new resource for these commodities.

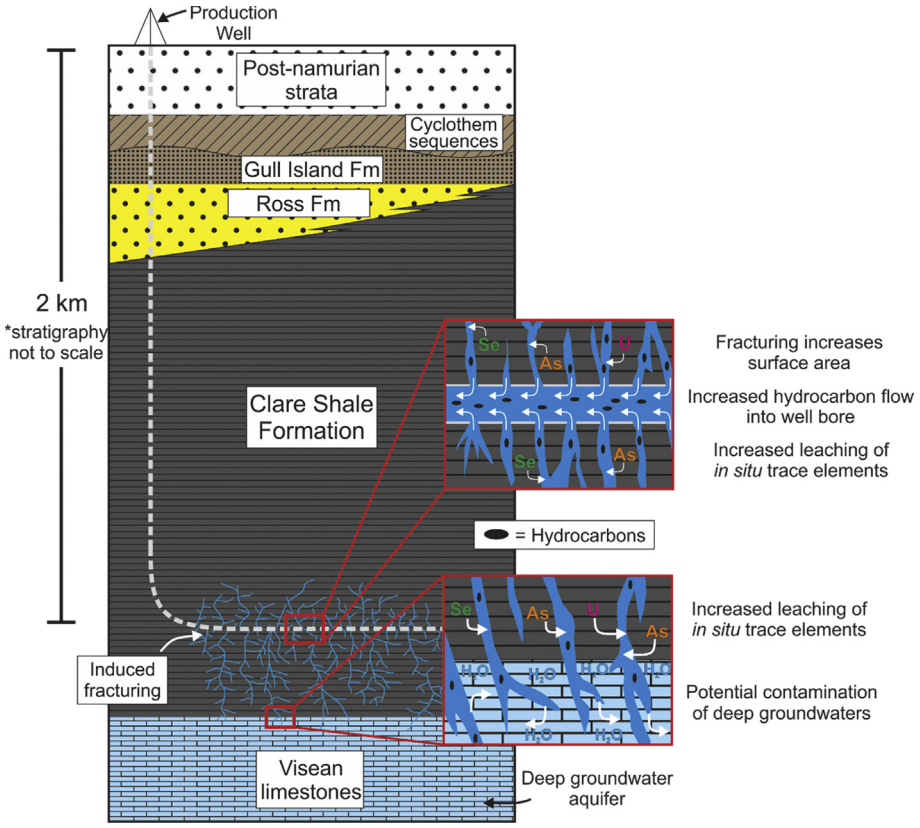

Fig. 10. Example diagram of hydraulic fracturing processes, utilising generalised Irish Namurian stratigraphy (Fig. 1). Sites of potential trace element leaching and water contamination are highlighted.

6. Conclusions

Identifying enrichments of trace elements in ancient and modern sedimentary environments is key to understanding wider trace element cycling in the upper crust. The key findings of this work can be split into two categories, with wider implication associated with each; Carboniferous deep marine black shales across the British Isles have consistently elevated concentrations of redox sensitive trace elements; Oxic groundwater precipitates associated with the Carboniferous shales contains elevated, but variable, As, Cu, Se, Tl, U and V concentrations.

Elevated levels of redox sensitive trace elements within Carboniferous black shales indicate:

1. Widespread deep marine basin deposition during the Namurian under prolonged anoxic-euxinic conditions, likely within stratified sub-basins.
2. Trace element concentrations were elevated within global oceans during the Carboniferous, correlatable with the rapid rise in global atmospheric oxygen levels during this time.
3. Increased oxidative weathering of the continental crust may have resulted in a higher flux of trace elements to ocean basins during the Carboniferous and at other times of atmospheric oxygenation.

The observed oxidative weathering and groundwater leaching of Carboniferous shales demonstrates the following:

1. Many trace elements within these deep marine black shales can be mobilised by groundwater under ambient surface oxidising conditions.
2. Leaching groundwaters can form enriched Fe-rich oxide precipitates when exposed at surface. Abundant trace element fixation can occur in areas of secondary oxide mineralisation. This process is very comparable to AMD formation observed at abandoned mining sites.
3. Selenium and As preferentially substitute into partially phosphatic, rather than sulphatic jarosite species or iron oxides in this system. This has implications for AMD site remediation and the identification of secondary trace element accumulations. This finding could result in improved methods of AMD management, through the intentional formation of phosphatic oxide species for selective trace element fixation.

Finally, the demonstrated oxidation and mobilisation of potentially hazardous trace elements from organic-rich black shales has significant environmental implications for the induced fracturing of shales. This work suggests that contamination of produced and natural waters may occur as a result of elemental leaching from *in situ* black shale formations. The increased surface area of black shales after fracturing could result in increased leaching rates into associated groundwaters, similar to AMD formation from abandoned coal mines, potentially catalysed by the use of acids during the induced fracturing process. Leaching processes could be delayed until hydrocarbon extraction ceases and groundwater equilibrium is re-established, however reduced groundwater conditions may limit the chemical breakdown and leaching of shale formations.

These observations should be considered when evaluating the environmental impact and potential remediation costs associated with elemental leaching during induced hydraulic fracturing. However, with the increasing demand for critical trace elements such as Se, Te and Co, the observed leaching processes could provide a new resource as a by-product from produced waters.

Acknowledgements

We would like to thank John Still and Alison McDonald for their skilled technical support. Robert Thorne and one other reviewer are thanked for their helpful comments.

Funding: This work was supported by NERC, UK [grant numbers NE/M010953/1, IP-1631-0516]. AJB is funded by NERC support of the Isotope Community Support Facility SUERC.

Appendix A. Supplementary data

Supplementary data to this article can be found online at https://doi.org/10.1016/j.apgeochem.2019.104401.

References

Acero, P., Ayora, C., Torrentó, C., Nieto, J.M., 2006. The behavior of trace elements during schwertmannite precipitation and subsequent transformation into goethite and jarosite. Geochem. Cosmochim. Acta 70, 4130–4139. https://doi.org/10.1016/j.gca.2006.06.1367.

Andrews, I.J., 2013. The Carboniferous Bowland Shale Gas Study: Geology and Resource Estimation. Department for Energy and Climate Change, London. https://doi.org/10.1080/10962247.2014.897270.

Armstrong, J.G.T., Parnell, J., Bullock, L.A., Perez, M., Boyce, A.J., Feldmann, J., 2018. Tellurium, selenium and cobalt enrichment in Neoproterozoic black shales, Gwna Group, UK: deep marine trace element enrichment during the Second Great Oxygenation Event. Terra. Nova 30, 244–253. https://doi.org/10.1111/ter.12331.

Asta, M.P., Cama, J., Martínez, M., Giménez, J., 2009. Arsenic removal by goethite and jarosite in acidic conditions and its environmental implications. J. Hazard Mater. 171, 965–972. https://doi.org/10.1016/j.jhazmat.2009.06.097.

Bajwa, B.S., Kumar, S., Singh, S., Sahoo, S.K., Tripathi, R.M., 2017. Uranium and other heavy toxic elements distribution in the drinking water samples of SW-Punjab, India. J. Radiat. Res. Appl. Sci. 10, 13–19. https://doi.org/10.1016/j.jrras.2015.01.002.

Balaba, R.S., Smart, R.B., 2012. Total arsenic and selenium analysis in Marcellus shale, high-salinity water, and hydrofracture flowback wastewater. Chemosphere 89, 1437–1442. https://doi.org/10.1016/j.chemosphere.2012.06.014.

Balistrieri, L.S., Chao, T.T., 1987. Selenium adsorption by goethite. Soil Sci. Soc. Am. J. 51, 1145–1151.

Baron, D., Palmer, C.D., 1996. Solubility of $KFe_3(CrO_4)2(OH)_6$ at 4 to 35°C. Geochem. Cosmochim. Acta 60, 3815–3824. https://doi.org/10.1016/0016-7037(96)00206-2.

Baruah, B.P., Khare, P., 2010. Mobility of trace and potentially harmful elements in the environment from high sulfur Indian coal mines. Appl. Geochem. 25, 1621–1631. https://doi.org/10.1016/j.apgeochem.2010.08.010.

Böttcher, M.E., Brumsack, H.-J., Dürselen, C.-D., 2007. The isotopic composition of modern seawater sulfate: I. Coastal waters with special regard to the North Sea. J. Mar. Syst. 67, 73–82. https://doi.org/10.1016/j.jmarsys.2006.09.006.

Breit, G.N., Wanty, R.B., 1991. Vanadium accumulation in carbonaceous rocks: a review of geochemical controls during deposition and diagenesis. Chem. Geol. 91, 83–97. https://doi.org/10.1016/0009-2541(91)90083-4.

Bullock, L., Parnell, J., Perez, M., Feldmann, J., Armstrong, J., 2017. Selenium and other trace element mobility in waste products and weathered sediments at parys mountain copper mine, anglesey. UK. Miner. 7, 229. https://doi.org/10.3390/min7110229.

Bullock, L.A., Perez, M., Armstrong, J.G., Parnell, J., Still, J., Feldmann, J., 2018. Selenium and tellurium resources in Kisgruva Proterozoic volcanogenic massive sulphide deposit (Norway). Ore Geol. Rev. 99, 411–424. https://doi.org/10.1016/j.oregeorev.2018.06.023.

Calvert, S., Pedersen, T., 1993. Geochemistry of Recent oxic and anoxic marine sediments: implications for the geological record. Mar. Geol. 113, 67–88. https://doi.org/10.1016/0025-3227(93)90150-T.

Campbell, I.H., Squire, R.J., 2010. The mountains that triggered the late neoproterozoic increase in oxygen: the second great oxidation event. Geochem. Cosmochim. Acta 74, 4187–4206. https://doi.org/10.1016/j.gca.2010.04.064.

Canfield, D.E., Poulton, S.W., Knoll, A.H., Narbonne, G.M., Ross, G., Goldberg, T., Strauss, H., 2008. Ferruginous conditions dominated later neoproterozoic deep-water chemistry. Science 321, 949–952. (80-.). https://doi.org/10.1126/science.1154499.

Cary, L., Benabderraziq, H., Elkhattabi, J., Gourcy, L., Parmentier, M., Picot, J., Khaska, M., Laurent, A., Négrel, P., 2014. Tracking selenium in the Chalk aquifer of northern France: Sr isotope constraints. Appl. Geochem. 48, 70–82. https://doi.org/10.1016/j.apgeochem.2014.07.014.

Centner, T.J., 2013. Oversight of shale gas production in the United States and the disclosure of toxic substances. Resour. Policy 38, 233–240. https://doi.org/10.1016/j.resourpol.2013.03.001.

Chappaz, A., Lyons, T.W., Gregory, D.D., Reinhard, C.T., Gill, B.C., Li, C., Large, R.R., 2014. Does pyrite act as an important host for molybdenum in modern and ancient euxinic sediments? Geochem. Cosmochim. Acta 126, 112–122. https://doi.org/10.1016/j.gca.2013.10.028.

Chelvanathan, P., Hossain, M.I., Amin, N., 2010. Performance analysis of copper–-indium–gallium–diselenide (CIGS) solar cells with various buffer layers by SCAPS. Curr. Appl. Phys. 10, S387–S391. https://doi.org/10.1016/j.cap.2010.02.018.

Collinson, J.D., Martinsen, O., Bakken, B., Kloster, A., 1991. Early fill of the Western Irish Namurian Basin: a complex relationship between turbidites and deltas. Basin Res. 3, 223–242. https://doi.org/10.1111/j.1365-2117.1991.tb00131.x.

Crusius, J., Calvert, S., Pedersen, T., Sage, D., 1996. Rhenium and molybdenum enrichments in sediments as indicators of oxic, suboxic and sulfidic conditions of deposition. Earth Planet. Sci. Lett. 145, 65–78. https://doi.org/10.1016/S0012-821X(96)00204-X.

Cucchiella, F., D'Adamo, I., Lenny Koh, S.C., Rosa, P., 2015. Recycling of WEEEs: an economic assessment of present and future e-waste streams. Renew. Sustain. Energy Rev. 51, 263–272. https://doi.org/10.1016/j.rser.2015.06.010.

Dang, Z., Liu, C., Haigh, M.J., 2002. Mobility of heavy metals associated with the natural weathering of coal mine spoils. Environ. Pollut. 118, 419–426. https://doi.org/10.1016/S0269-7491(01)00285-8.

Descostes, M., Vitorge, P., Beaucaire, C., 2004. Pyrite dissolution in acidic media. Geochem. Cosmochim. Acta 68, 4559–4569. https://doi.org/10.1016/j.gca.2004.04.012.

Dutrizac, J.E., Chen, T.T., 2010. The behaviour of phosphate during jarosite precipitation. Hydrometallurgy 102, 55–65. https://doi.org/10.1016/j.hydromet.2010.02.004.

Dutrizac, J.E., Dinardo, O., Kaiman, S., 1981. Selenate analogues of jarosite-type compounds. Hydrometallurgy 6, 327–337. https://doi.org/10.1016/0304-386X(81)90049-9.

Eftekhari, A., 2017. The rise of lithium–selenium batteries. Sustain. Energy Fuels 1, 14–29. https://doi.org/10.1039/C6SE00094K.

Fontenot, B.E., Hunt, L.R., Hildenbrand, Z.L., Carlton Jr., D.D., Oka, H., Walton, J.L., Hopkins, D., Osorio, A., Bjorndal, B., Hu, Q.H., Schug, K.A., 2013. An evaluation of water quality in private drinking water wells near natural gas extraction sites in the Barnett shale formation. Environ. Sci. Technol. 47, 10032–10040. https://doi.org/10.1021/es4011724.

Francis, J.G., Ryback, G., 1987. Chalcomenite from ballybunnion, Co. Kerry, eire. Mineral. Mag. 51, 751–752.

Gallazzi, D., 2012. Shale gas hydraulic fracturing in Ireland. In: Proceedings of the 32nd Annual Groundwater Conference. International Association of Hydrogeologists (Irish Group), Tullamore, Co Offaly 1:21-1:28.

Gardiner, P.R.R., MacCarthy, I.A.J., 1981. The Late Paleozoic evolution of southern Ireland in the context of tectonic basins and their transatlantic significance. Can. Soc. Pet. Geol. 7, 683–725.

Goodhue, R., Clayton, G., 1999. Organic maturation levels, thermal history and hydrocarbon source rock potential of the Namurian rocks of the Clare Basin, Ireland. Mar. Pet. Geol. 16, 667–675. https://doi.org/10.1016/S0264-8172(99)00016-1.

Grenthe, I., Stumm, W., Laaksuharju, M., Nilsson, A.C., Wikberg, P., 1992. Redox potentials and redox reactions in deep groundwater systems. Chem. Geol. 98, 131–150. https://doi.org/10.1016/0009-2541(92)90095-M.

Guo, T., Li, Y., Ding, Y., Qu, Z., Gai, N., Rui, Z., 2017. Evaluation of acid fracturing treatments in shale formation. Energy Fuels 31, 10479–10489. https://doi.org/10.1021/acs.energyfuels.7b01398.

Hakonson-Hayes, A., Fresquez, P., Whicker, F., 2002. Assessing potential risks from exposure to natural uranium in well water. J. Environ. Radioact. 59, 29–40. https://doi.org/10.1016/S0265-931X(01)00034-0.

Hall, A.J., Boyce, A.J., Fallick, A.E., 1994. A sulphur isotope study of iron sulphides in the late Precambrian Dalradian Ardrishaig Phyllite Formation, Knapdale, Argyll. Scottish J. Geol. 30, 63–71.

He, B., Liang, L., Jiang, G., 2002. Distributions of arsenic and selenium in selected Chinese coal mines. Sci. Total Environ. 296, 19–26.

Hu, Z., Gao, S., 2008. Upper crustal abundances of trace elements: a revision and update. Chem. Geol. 253, 205–221. https://doi.org/10.1016/j.chemgeo.2008.05.010.

Huyen, D.T., Tabelin, C.B., Thuan, H.M., Dang, D.H., Truong, P.T., Vongphuthone, B., Kobayashi, M., Igarashi, T., 2019. The solid-phase partitioning of arsenic in unconsolidated sediments of the Mekong Delta, Vietnam and its modes of release under various conditions. Chemosphere 233, 512–523. https://doi.org/10.1016/j.chemosphere.2019.05.235.

Islam, M.R., Salminen, R., Lahermo, P.W., 2000. Arsenic and other toxic elemental contamination of groundwater, surface water and soil in Bangladesh and its possible effects on human health. Environ. Geochem. Health 22, 33–53. https://doi.org/10.1023/A:1006787405626.

Jacobson, A.T., Fan, M., 2019. Evaluation of natural goethite on the removal of arsenate and selenite from water. J. Environ. Sci. 76, 133–141. https://doi.org/10.1016/j.jes.2018.04.016.

Johnson, D.B., Hallberg, K.B., 2005. Acid mine drainage remediation options: a review. Sci. Total Environ. 338, 3–14. https://doi.org/10.1016/j.scitotenv.2004.09.002.

Jones, B., Manning, D.A.C., 1994. Comparison of geochemical indices used for the interpretation of palaeoredox conditions in ancient mudstones. Chem. Geol. 111, 111–129. https://doi.org/10.1016/0009-2541(94)90085-X.

Jones, G.L., 2012. Hydraulic fracturing for shale gas in Ireland - the potential. In: Proceedings of the 32nd Annual Groundwater Conference. International Association of Hydrogeologists (Irish Group), Tullamore, Co Offaly 1:13-1:20.

Jones, P.C., Naylor, D., 2003. Namurian rocks of Whiddy Island, west cork: a sedimentological outline and palaeogeographical implications. Ir. J. Earth Sci. 21, 115–132.

Kampschulte, A., Strauss, H., 2004. The sulfur isotopic evolution of Phanerozoic seawater based on the analysis of structurally substituted sulfate in carbonates. Chem. Geol. 204, 255–286. https://doi.org/10.1016/j.chemgeo.2003.11.013.

Large, R.R., Halpin, J.A., Danyushevsky, L.V., Maslennikov, V.V., Bull, S.W., Long, J.A., Gregory, D.D., Lounejeva, E., Lyons, T.W., Sack, P.J., McGoldrick, P.J., Calver, C.R., 2014. Trace element content of sedimentary pyrite as a new proxy for deep-time ocean–atmosphere evolution. Earth Planet. Sci. Lett. 389, 209–220. https://doi.org/10.1016/j.epsl.2013.12.020.

Large, R.R., Halpin, J.A., Lounejeva, E., Danyushevsky, L.V., Maslennikov, V.V., Gregory, D., Sack, P.J., Haines, P.W., Long, J.A., Makoundi, C., Stepanov, A.S., 2015. Cycles of nutrient trace elements in the Phanerozoic ocean. Gondwana Res. 28, 1282–1293. https://doi.org/10.1016/j.gr.2015.06.004.

Large, R.R., Mukherjee, I., Gregory, D., Steadman, J., Corkrey, R., Danyushevsky, L.V., 2019. Atmosphere oxygen cycling through the proterozoic and phanerozoic. Miner. Depos. 54, 485–506. https://doi.org/10.1007/s00126-019-00873-9.

Large, R.R., Mukherjee, I., Gregory, D.D., Steadman, J.A., Maslennikov, V.V., Meffre, S., 2017. Ocean and atmosphere geochemical proxies derived from trace elements in marine pyrite: implications for ore genesis in sedimentary basins. Econ. Geol. 112, 423–450. https://doi.org/10.2113/econgeo.112.2.423.

Lee, J.S., Chon, H.T., Kim, J.S., Kim, K.W., Moon, H.S., 1998. Enrichment of potentially toxic elements in areas underlain by black shales and slates in Korea. Environ. Geochem. Health 20, 135–147. https://doi.org/10.1023/A:1006571223295.

Leite, D. da S., Carvalho, P.L.G., de Lemos, L.R., Mageste, A.B., Rodrigues, G.D., 2017. Hydrometallurgical separation of copper and cobalt from lithium-ion batteries using

aqueous two-phase systems. Hydrometallurgy 169, 245–252. https://doi.org/10.1016/j.hydromet.2017.01.002.
Li, M., Wei, C., Qiu, S., Zhou, X., Li, C., Deng, Z., 2010. Kinetics of vanadium dissolution from black shale in pressure acid leaching. Hydrometallurgy 104, 193–200. https://doi.org/10.1016/j.hydromet.2010.06.001.
Lipinski, M., Warning, B., Brumsack, H.-J., 2003. Trace metal signatures of jurassic/cretaceous black shales from the Norwegian shelf and the barents sea. Palaeogeogr. Palaeoclimatol. Palaeoecol. 190, 459–475. https://doi.org/10.1016/S0031-0182(02)00619-3.
Liu, H., Shi, Z., Li, J., Zhao, P., Qin, S., Nie, Z., 2018. The impact of phosphorus supply on selenium uptake during hydroponics experiment of winter wheat (Triticum aestivum) in China. Front. Plant Sci. 9, 1–9. https://doi.org/10.3389/fpls.2018.00373.
Luning, S., Kolonic, S., 2003. Uranium spectral gamma-ray response as a proxy for organic richness in black shales: applicability and limitations. J. Pet. Geol. 26, 153–174. https://doi.org/10.1111/j.1747-5457.2003.tb00023.x.
Martinsen, O.J., Pulham, A.J., Elliott, T., Haughton, P., Pierce, C., Lacchia, A.R., Barker, S., Latre, A.O., Kane, I., Shannon, P., Sevastopulo, G.D., 2017. Deep-water clastic systems in the upper carboniferous (upper mississippian–lower pennsylvanian) shannon basin, western Ireland. Am. Assoc. Petrol. Geol. Bull. 101, 433–439. https://doi.org/10.1306/021417DIG17099.
McHugh, T., Molofsky, L., Daus, A., Connor, J., 2014. Comment on “an evaluation of water quality in private drinking water wells near natural gas extraction sites in the Barnett shale formation. Environ. Sci. Technol. 48, 3595–3596. https://doi.org/10.1021/es405772d.
Menning, M., Alekseev, A.S., Chuvashov, B.I., Davydov, V.I., Devuyst, F.-X., Forke, H.C., Grunt, T.A., Hance, L., Heckel, P.H., Izokh, N.G., Jin, Y.-G., Jones, P.J., Kotlyar, G.V., Kozur, H.W., Nemyrovska, T.I., Schneider, J.W., Wang, X.-D., Weddige, K., Weyer, D., Work, D.M., 2006. Global time scale and regional stratigraphic reference scales of central and west europe, East europe, tethys, south China, and North America as used in the devonian–carboniferous–permian correlation chart 2003 (DCP 2003). Palaeogeogr. Palaeoclimatol. Palaeoecol. 240, 318–372. https://doi.org/10.1016/j.palaeo.2006.03.058.
Moncaster, S.J., Bottrell, S.H., Tellam, J.H., Lloyd, J.W., Konhauser, K.O., 2000. Migration and attenuation of agrochemical pollutants: insights from isotopic analysis of groundwater sulphate. J. Contam. Hydrol. 43, 147–163.
Morales-Acevedo, A., 2006. Thin film CdS/CdTe solar cells: research perspectives. Sol. Energy 80, 675–681. https://doi.org/10.1016/j.solener.2005.10.008.
Moreton, S., Ryback, G., Aspen, P., 1995. Basaluminite, hydronium jarosite, metasideronatrite and sideronatrite. Four sulphate minerals new to Ireland: from ballybunnion, county kerry. Ir. J. Earth Sci. 14, 1–5.
Nolan, K., 2012. The Clare Shale Formation, West Ireland: the Sedimentological Variability of a Potential Shale Gas Reservoir. University of Manchester.
Novak, M., Bottrell, S.H., Pirechova, E.V.A., 2001. Sulfur isotope inventories of atmospheric deposition, spruce floor and living Sphanum along a NW-SE transect across Europe. Biogeochemistry 53, 23–50.
Osborn, S.G., Vengosh, A., Warner, N.R., Jackson, R.B., 2011. Methane contamination of drinking water accompanying gas-well drilling and hydraulic fracturing. Proc. Natl. Acad. Sci. 108, 8172–8176. https://doi.org/10.1073/pnas.1100682108.
Paikaray, S., 2012. Environmental hazards of arsenic associated with black shales: a review on geochemistry, enrichment and leaching mechanism. Rev. Environ. Sci. Bio.Technol. 11, 289–303. https://doi.org/10.1007/s11157-012-9281-z.
Paktunc, D., Dutrizac, J.E., 2003. Characterization of arsenate-for-sulfate substitution in synthetic jarosite using x-ray diffraction and x-ray absorption spectroscopy. Can. Mineral. 41, 905–919. https://doi.org/10.2113/gscanmin.41.4.905.
Parnell, J., Brolly, C., Spinks, S., Bowden, S., 2016. Selenium enrichment in Carboniferous Shales, Britain and Ireland: problem or opportunity for shale gas extraction? Appl. Geochem. 66, 82–87. https://doi.org/10.1016/j.apgeochem.2015.12.008.
Parnell, J., Bullock, L., Armstrong, J., Perez, M., 2018. Liberation of selenium from alteration of the Bowland shale formation: evidence from the mam tor landslide. Q. J. Eng. Geol. Hydrogeol. 51, 503–508. https://doi.org/10.1144/qjegh2018-026.
Peters, S.C., Burkert, L., 2008. The occurrence and geochemistry of arsenic in groundwaters of the Newark basin of Pennsylvania. Appl. Geochem. 23, 85–98. https://doi.org/10.1016/j.apgeochem.2007.10.008.
Pollastro, R.M., Jarvie, D.M., Hill, R.J., Adams, C.W., 2007. Geologic framework of the mississippian Barnett shale, barnett-paleozoic total petroleum system, bend arch–fort worth basin, Texas. Am. Assoc. Petrol. Geol. Bull. 91, 405–436. https://doi.org/10.1306/10300606008.
Raiswell, R., Canfield, D.E., 1998. Sources of iron for pyrite formation in marine sediments. Am. J. Sci. 298, 219–245.
Renock, D., Landis, J.D., Sharma, M., 2016. Reductive weathering of black shale and release of barium during hydraulic fracturing. Appl. Geochem. 65, 73–86. https://doi.org/10.1016/j.apgeochem.2015.11.001.
Rider, M.H., 1974. The namurian of west county Clare. Proc. Irish Acad. Sect. B Biol. Geol. Chem. Sci. 74, 125–142.
Rimstidt, J.D., Chermak, J.A., Schreiber, M.E., 2017. Processes that control mineral and element abundances in shales. Earth Sci. Rev. 171, 383–399. https://doi.org/10.1016/j.earscirev.2017.06.010.
Robinson, B.W., Kusakabe, M., 1975. Quantitative preparation of sulfur dioxide, for $^{34}S/^{32}S$ analyses, from sulfides by combustion with cuprous oxide. Anal. Chem. 47, 1179–1181. https://doi.org/10.1021/ac60357a026.
Rudnick, R.L., Gao, S., 2003. Composition of the continental crust. In: Holland, H.D., Turekian, K.K. (Eds.), Treatise on Geochemistry. Elsevier B.V., pp. 1–64.
Rumsey, M.S., 2016. The first occurrence of mandarinoite, $Fe_2(SeO_3)_3.6H_2O$, in the British Isles, from cliffs near Ballybunion, Co. Kerry, Ireland. J. Russell Soc. 19, 35–38.
Scott, C., Lyons, T.W., 2012. Contrasting molybdenum cycling and isotopic properties in euxinic versus non-euxinic sediments and sedimentary rocks: refining the paleoproxies. Chem. Geol. 324–325, 19–27. https://doi.org/10.1016/j.chemgeo.2012.05.012.
Settari, A., 1980. Simulation of hydraulic fracturing processes. Soc. Pet. Eng. J. 20, 487–500. https://doi.org/10.2118/7693-PA.
Sheoran, A.S., Sheoran, V., 2006. Heavy metal removal mechanism of acid mine drainage in wetlands: a critical review. Miner. Eng. 19, 105–116. https://doi.org/10.1016/j.mineng.2005.08.006.
Smedley, P.L., Kinniburgh, D.G., 2002. A_review_of_the_source_behaviour_and_dis.pdf. pp. 517–568. 17. https://doi.org/10.1016/S0883-2927(02)00018-5.
Strawn, D., Doner, H., Zavarin, M., McHugo, S., 2002. Microscale investigation into the geochemistry of arsenic, selenium, and iron in soil developed in pyritic shale materials. Geoderma 108, 237–257. https://doi.org/10.1016/S0016-7061(02)00133-7.
Stüeken, E.E., Buick, R., Bekker, A., Catling, D., Foriel, J., Guy, B.M., Kah, L.C., Machel, H.G., Montañez, I.P., Poulton, S.W., 2015a. The evolution of the global selenium cycle: secular trends in Se isotopes and abundances. Geochem. Cosmochim. Acta 162, 109–125. https://doi.org/10.1016/j.gca.2015.04.033.
Stüeken, E.E., Foriel, J., Buick, R., Schoepfer, S.D., 2015b. Selenium isotope ratios, redox changes and biological productivity across the end-Permian mass extinction. Chem. Geol. 410, 28–39. https://doi.org/10.1016/j.chemgeo.2015.05.021.
Swanner, E.D., Planavsky, N.J., Lalonde, S.V., Robbins, L.J., Bekker, A., Rouxel, O.J., Saito, M.A., Kappler, A., Mojzsis, S.J., Konhauser, K.O., 2014. Cobalt and marine redox evolution. Earth Planet. Sci. Lett. 390, 253–263. https://doi.org/10.1016/j.epsl.2014.01.001.
Tabelin, C.B., Hashimoto, A., Igarashi, T., Yoneda, T., 2014. Leaching of boron, arsenic and selenium from sedimentary rocks: I. Effects of contact time, mixing speed and liquid-to-solid ratio. Sci. Total Environ. 472, 620–629. https://doi.org/10.1016/j.scitotenv.2013.11.006.
Tabelin, C.B., Igarashi, T., Villacorte-Tabelin, M., Park, I., Opiso, E.M., Ito, M., Hiroyoshi, N., 2018. Arsenic, selenium, boron, lead, cadmium, copper, and zinc in naturally contaminated rocks: a review of their sources, modes of enrichment, mechanisms of release, and mitigation strategies. Sci. Total Environ. 645, 1522–1553. https://doi.org/10.1016/j.scitotenv.2018.07.103.
Tabelin, C.B., Sasaki, R., Igarashi, T., Park, I., Tamoto, S., Arima, T., Ito, M., Hiroyoshi, N., 2017. Simultaneous leaching of arsenite, arsenate, selenite and selenate, and their migration in tunnel-excavated sedimentary rocks: I. Column experiments under intermittent and unsaturated flow. Chemosphere 186, 558–569. https://doi.org/10.1016/j.chemosphere.2017.07.145.
Tanner, D.C., Bense, F.A., Ertl, G., 2011. Kinematic retro-modelling of a cross-section through a thrust-and-fold belt: the Western Irish Namurian Basin. Geol. Soc. London Spec. Publ. 349, 61–76. https://doi.org/10.1144/SP349.4.
Turekian, K.K., Wedepohl, K.H., 1961. Distribution of the elements in some major units of the earth's crust. Geol. Soc. Am. Bull. 72, 175–192.
Tuttle, M.L.W., Fahy, J.W., Elliott, J.G., Grauch, R.I., Stillings, L.L., 2014a. Contaminants from Cretaceous black shale: I. Natural weathering processes controlling contaminant cycling in Mancos Shale, southwestern United States, with emphasis on salinity and selenium. Appl. Geochem. 46, 57–71. https://doi.org/10.1016/j.apgeochem.2013.12.010.
Tuttle, M.L.W., Fahy, J.W., Elliott, J.G., Grauch, R.I., Stillings, L.L., 2014b. Contaminants from cretaceous black shale: II. Effect of geology, weathering, climate, and land use on salinity and selenium cycling, Mancos Shale landscapes, southwestern United States. Appl. Geochem. 46, 72–84. https://doi.org/10.1016/j.apgeochem.2013.12.011.
Vengosh, A., Jackson, R.B., Warner, N., Darrah, T.H., Kondash, A., 2014. A critical review of the risks to water resources from unconventional shale gas development and hydraulic fracturing in the United States. Environ. Sci. Technol. 48, 8334–8348. https://doi.org/10.1021/es405118y.
Wayland, M., Crosley, R., 2006. Selenium and other trace elements in aquatic insects in coal mine–affected streams in the rocky mountains of alberta, Canada. Arch. Environ. Contam. Toxicol. 50, 511–522. https://doi.org/10.1007/s00244-005-0114-8.
Wignall, P.B., Best, J.L., 2000. The western Irish namurian basin reassessed. Basin Res. 12, 59–78.
Williams, E.A., 2000. Flexural cantilever models of extensional subsidence in the Munster Basin (SW Ireland) and Old Red Sandstone fluvial dispersal systems. Geol. Soc. London Spec. Publ. 180, 239–268. https://doi.org/10.1144/GSL.SP.2000.180.01.12.
Xiao, T., Yang, F., Li, S., Zheng, B., Ning, Z., 2012. Thallium pollution in China: a geo-environmental perspective. Sci. Total Environ. 421–422, 51–58. https://doi.org/10.1016/j.scitotenv.2011.04.008.
Xu, G., Hannah, J.L., Bingen, B., Georgiev, S., Stein, H.J., 2012. Digestion methods for trace element measurements in shales: paleoredox proxies examined. Chem. Geol. 324–325, 132–147. https://doi.org/10.1016/j.chemgeo.2012.01.029.
Yang, S., Horsfield, B., Mahlstedt, N., Stephenson, M., Könitzer, S., 2016. On the primary and secondary petroleum generating characteristics of the Bowland Shale, northern England. J. Geol. Soc. London. 173, 292–305. https://doi.org/10.1144/jgs2015-056.
Zheng, B., Ding, Z., Huang, R., Zhu, J., Yu, X., Wang, A., Zhou, D., Mao, D., Su, H., 1999. Issues of health and disease relating to coal use in southwestern China. Int. J. Coal Geol. 40, 119–132. https://doi.org/10.1016/S0166-5162(98)00064-0.
Zheng, Y., Stute, M., van Geen, A., Gavrieli, I., Dhar, R., Simpson, H.J., Schlosser, P., Ahmed, K.M., 2004. Redox control of arsenic mobilization in Bangladesh groundwater. Appl. Geochem. 19, 201–214. https://doi.org/10.1016/j.apgeochem.2003.09.007.
Zhou, J., Yang, J., Xu, Z., Zhang, T., Chen, Z., Wang, J., 2017. A high performance lithium–selenium battery using a microporous carbon confined selenium cathode and a compatible electrolyte. J. Mater. Chem. 5, 9350–9357. https://doi.org/10.1039/C7TA01564J.